Bio-Physical Modeling of *Galvanic* Human Body Communication in Electro-Quasistatic Regime

Nirmoy Modak, Mayukh Nath, Baibhab Chatterjee, *Graduate Student Member, IEEE*, Shovan Maity, and Shreyas Sen, *Senior Member, IEEE*

***Abstract*—Human Body Communication (HBC) is an alternative to radio wave-based Wireless Body Area Network (WBAN) because of its wide bandwidth leading to enhanced energy efficiency. Designing Modern HBC devices need the accurate electrical equivalent of the HBC channel for energy efficient communication. The objective of this paper is to present an improved lumped element-based detailed model of Galvanic HBC channel which can be used to explain the dependency of the channel behaviour on the internal body dependent parameters such as electrical properties of skin and muscle tissue layers along with the external parameters such as electrode size, electrode separation, geometrical position of the electrodes and return-path or parasitic capacitances. The model considers the frequency-dependent impedance of skin and muscle tissue layers and the effect of various coupling capacitances between the body and Tx/Rx electrodes to the Earth-Ground. A 2D planar structure of skin and muscle tissue layers is simulated using a Finite Element Method (FEM) tool to prove the validity of the proposed model. The effect of *symmetry* and *asymmetry* at the transmitter and receiver ends is also explained using the model. The model become very useful for fast calculation of Galvanic channel response without using any FEM tool. Experimental results show that the galvanic response is not only a function of channel length but also depends on the mismatch at the transmitter and receiver end. In case of a very high mismatch scenario, the channel behavior is dominated by the capacitive HBC, even for a galvanic excitation and termination.**

***Index Terms*—Human body communication (HBC), body area network (BAN), channel modelling, galvanic HBC, biophysical circuit model.**

Manuscript received 26 November 2020; revised 6 April 2021, 30 June 2021, and 2 September 2021; accepted 13 October 2021. Date of publication 20 May 2022; date of current version 22 November 2022. This work was supported in part by the Air Force Office of Scientific Research YIP Award under Grant FA9550-17-1-0450, in part by the National Science Foundation CRII Award under Grant CNS 1657455, and in part by Eli Lilly and Company through the Connected Health care initiative. *(Corresponding author: Shreyas Sen.)*

Nirmoy Modak, Mayukh Nath, Baibhab Chatterjee, and Shovan Maity are with the School of Electrical and Computer Engineering, Purdue University, USA.

Shreyas Sen is with the School of Electrical and Computer Engineering, Purdue University, West Lafayette, IN 47907 USA (e-mail: shreyas@purdue.edu).

This article has supplementary downloadable material available at https://doi.org/10.1109/TBME.2022.3176541, provided by the authors.

Digital Object Identifier 10.1109/TBME.2022.3176541

I. Introduction

HUMAN Body Communication (HBC) was first introduced by Zimmerman [1] in 1995. It is gaining significant recognition in the field of continuous healthcare monitoring as well as in the field of Wearable and Implantable devices which use Body Area Network (BAN) for communication [2]–[5]. Wearable devices like ECG band, wristwatch, flexible electronics, etc. use BAN to collect the vital information continuously and generate appropriate signals whenever an anomaly is detected. Apart from this, those small and tiny sensors do not restrict body movements which allow the acquisition of biomedical signals uninterruptedly increasing the duration of operation without degrading the comfort level of a patient. High-Security level and data privacy are a few additional advantages which make it popular like Bluetooth network [6], [7]. In any communication method, an in-depth understanding of the channel-model is crucial for efficient circuits and systems development. While recently there have been a few Bio-Physical models developed for Capacitive HBC [8], [9] and Galvanic HBC [10]–[14], there is some room for improvement the Galvanic HBC channel model considering the simultaneous effect of parasitic capacitances and body impedance. Therefore, modeling the Galvanic HBC channel with the inclusion of parasitic or return-path capacitances is a strong open need in the field of the Human Body Communication.

In case of Capacitive HBC [Fig. 1(a)], the signal electrode of the transmitter is connected to the body with ground electrode floating [1]. The injected signal is sensed using a receiver connected somewhere else to the body in a similar fashion. The floating electrodes of the Transmitter or Receiver pair are coupled with the Earth-ground and form a return path for signal whereas the body provides the forward signal path. The path loss of Capacitive HBC is mostly determined by the return path capacitances and load capacitance due to the low impedance forward path through the body as described in [8].

Data transfer through human body using Galvanic HBC first proposed by Wegmueller [10] in 2010. Unlike Capacitive HBC, Galvanic HBC [Fig. 1(b)] uses a pair of electrodes to inject differential signal into the body. At the receiver side, another pair of electrodes receive the signal. Electrode size, electrode to the Earth-ground parasitic capacitances and the body channel length play a crucial role to define the overall galvanic channel characteristics. As both the Tx-Rx electrode pairs stay in contact with body, Galvanic HBC forms a more complex return

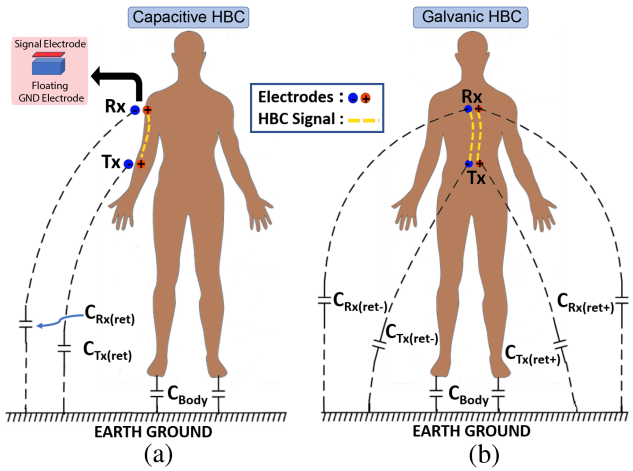

Fig. 1. HBC coupling modalities: (a) Capacitive (b) Galvanic.

path for signal compared to the Capacitive HBC as shown in the Fig. 1(b).

In this paper, we proposed a lumped element-based Bio-physical circuit model of Galvanic HBC considering the electrical parameters of skin and muscle tissue layers along with the return path capacitances associated to each of the electrodes. The model itself takes care of the geometric position of the electrodes which helps to understand the short channel and long channel response in a better way. The proposed model helps to improve the accuracy in predicting the transmitted and received signal under multiple scenarios. During the analysis, we have considered a planar structure of thin skin tissue layer on top of a thicker muscle tissue layer. The frequency dependent properties such as dielectric constant, conductivity, loss tangent, etc. of the above-mentioned layers are considered from [15] and [16]. Finite Element Analysis (FEA) results and the actual HBC channel response at multiple frequencies with different channel lengths are used to validate the proposed model and its accuracy.

The rest of the paper is organized as follows: Section II, discusses the background of HBC and compares some previous HBC channel measurement studies. The Bio-physical model of Galvanic HBC is derived in Section III. Section IV formulates the channel response expression considering a symmetric(or balanced) scenario at the transmitter and receiver side. Section V discusses the channel response considering asymmetry(or unbalanced) at the transmitter and/or receiver side. Section VI extends the concept of Section IV and V to a cylindrical model. Section VII contains the measurement setup and results. Section VIII discusses the measurement results and Section IX concludes the paper.

II. Background

The concept of Galvanic HBC was first introduced by Wegmueller [10] in 2010. Wegmueller showed that, the coupling of the signal to the human body can be done differentially using a pair of electrodes at transmitter side and another electrode pair can be used to acquire the signal differentially at the receiver side. Many studies have been carried out since then to characterize the Galvanic HBC channel and its loss. Electro Quasi-statics (EQS) Approximation [17], [18], Finite Element Analysis (FEA) [19]–[22], Finite Difference Time Domain Method (FDTD) [23], [24], Parametric Computational Analysis [25] and Equivalent Circuit Analysis (ECA) [12], [26]–[30] are the most popular methods used in the modelling of HBC channel. The EQS techniques are computationally fast and can be used for low- to mid-frequency range [31]. The Electrical Field analysis methods such as FDTD and FEA are accurate but need extensive tool-based simulation which is time consuming and not suitable for fast deployment of an IBN. On the other hand, ECA model deals with transfer function valid for a wide range of frequency with fast computing capability. In ECA approach, the studies conducted so far characterize the human body channel based on overall body impedance. Studies have been conducted considering single layer tissue-based model [10], [12], [28], multi-layer tissue-based model [13] and multi-layer tissue-based model [14] with bidirectional (longitudinal and cross paths) signal propagation can represent the behaviour of the channel, but those models are not suitable to explain the external dependencies (such as parasitic capacitance and return path capacitance) simultaneously which are integral part of the HBC channel. The goal of this paper is to develop a Bio-Physical Model, which captures the important physical phenomenon observable in experiments and can intuitively explain them with a single model. We proposed a lumped element-based circuit model that can be used to estimate the galvanic HBC channel response considering internal parameters of the human body as well as the external parameters such as parasitic capacitance and return path capacitance. The paper also establishes the effect of the symmetry and asymmetry present at the transmitter and receiver side on galvanic channel response due to the mismatch in return path capacitances using the same proposed model.

III. Bio-Physical Model Development

In this section, we have shown the analysis to find the equivalent lumped circuit for the skin tissue layer, muscle tissue layer, and return path capacitance. A 2D planar structure with skin and muscle tissue layer is used for the analysis in HFSS FEM simulator. Although the human body is not 2D, this analysis helps to understand the behavior of the HBC channel in a simplistic way. Later on, we have extended the concept of planar structure to a more complex human body in Section VI. In summary, the progression is chosen to build an intuitive explanation step by step.

A. Equivalent Circuit for Skin and Fat Layer

Coupling of the HBC signal to the human body is mainly affected by the thickness and the dielectric properties of the skin and fat tissue layer. In the Electro-Quasistatic regime, due to the dielectric nature of the skin layer, the effective skin impedance can be expressed by the (1) [16].

$$Z_{skin} = R_{skin} || \frac{1}{sC_{skin}} \tag{1}$$

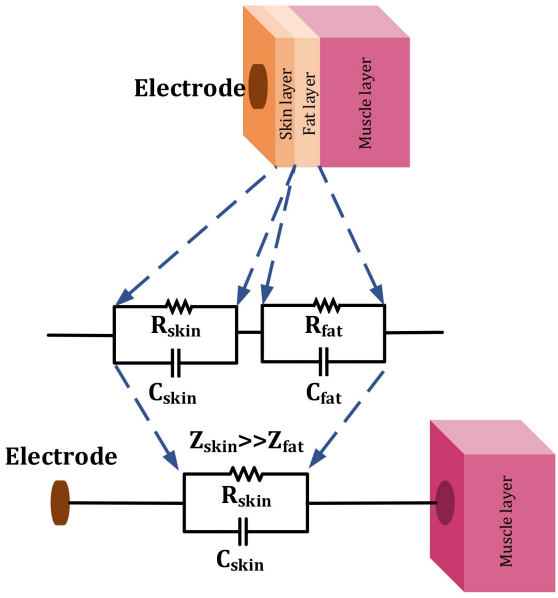

Fig. 2. Lumped circuit equivalent of the skin-flat layer.

where $R_{skin} = \frac{t_{skin}}{\sigma_{skin}.(\pi r^2)}$ is the skin resistance, $C_{skin} = \frac{\epsilon'_{skin}.(\pi r^2)}{t_{skin}}$ is the skin capacitance, ϵ'_{skin} is the absolute permittivity and σ_{skin} is the conductivity of the skin tissue layer at that frequency of operation [15]. Whereas, t_{skin} is the thickness of the skin tissue layer and r is the radius of the electrode connected.

Similar to the skin layer, the fat layer impedance also can be represented using a parallel combination of capacitance and resistance depending on the thickness and the dielectric properties of the fat at that frequency as shown in (2).

$$Z_{fat} = R_{fat} || \frac{1}{sC_{fat}} \tag{2}$$

The lumped circuit representation of the skin and fat layer for a particular electrode is shown in Fig. 2. Although we have shown the equivalent circuit model of skin and fat tissue layer, the experimental data [15], [16] show that up to 1 MHz frequency, the impedance of the fat tissue layer is much smaller than the impedance of the skin tissue layer. Therefore, if we neglect the fat tissue layer, the equivalent circuit reduces to a single RC network representing the skin properties and bridged between electrode and muscle tissue layer.

B. Equivalent Circuit for Muscle Layer

The transmitted current capacitively coupled to the muscle layer through the skin tissue layer. To find the current distribution in the muscle layer a planar muscle structure of finite thickness is considered as shown in Fig. 3. In EQS frequency regime, the portion of the muscle layer which is right below the electrode behave as an *equipotential surface* due to the highly conductive nature of muscle. For our analysis, we have considered two regions, *Region A* and *Region B* on the muscle layer which are right below the positive and negative transmitting electrodes respectively. Current *I*, which is coupled to the body through skin

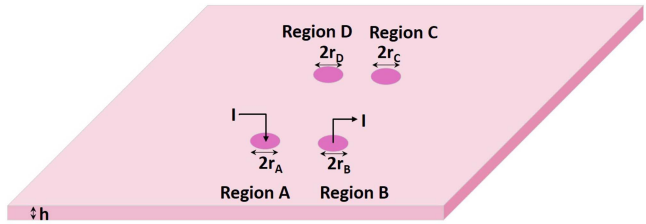

Fig. 3. A planar structure of muscle layer with coupled current I flowing from *Region A* to *Region B*.

tissue layer is flowing from *Region A* to *Region B*. *Region C* and *Region D* are the two regions on the muscle layer, right below the negative and positive electrode of the receiver. If the dimension of the muscle layer is higher than the electrode separation, the muscle tissue layer can be considered as an infinitely stretched conductor of thickness h_{muscle}. Now, as shown in Appendix A, the entire muscle tissue layer can be represented as a two-port network where the impedance (Z) parameters of the network are as follows:

$$Z_{11_{muscle}} = \frac{\rho_{muscle}}{2\pi h_{muscle}} \ln \left[\frac{r_{AB}}{r_A} \frac{r_{AB}}{r_B} \right] \tag{3}$$

$$Z_{12_{muscle}} = Z_{21_{muscle}} = \frac{\rho_{muscle}}{2\pi h_{muscle}} \ln \left[\frac{r_{AC}}{r_{AD}} \frac{r_{BD}}{r_{BC}} \right] \tag{4}$$

$$Z_{22_{muscle}} = \frac{\rho_{muscle}}{2\pi h_{muscle}} \ln \left[\frac{r_{CD}}{r_C} \frac{r_{CD}}{r_D} \right] \tag{5}$$

where $\rho_{muscle} (= 1/\sigma_{muscle})$ is the resistivity of the muscle tissue layer at that frequency of operation [15]; r_i (where i=A or B or C or D) is the radius of *Region i* and r_{ij} (where i or j =A or B or C or D) is the center to center distance between *Region i* and *Region j*.

The muscle layer can also be represented by using an impedance network as shown in Fig. 4. The impedance $Z_{T_{muscle}}$, $Z_{R_{muscle}}$ and $Z_{0_{muscle}}$ are the function of the impedance parameters $Z_{11_{muscle}}$, $Z_{12_{muscle}}$ and $Z_{22_{muscle}}$ as described by (6), (7) and (8).

$$\begin{aligned} Z_{T_{muscle}} &= \frac{1}{2} \left[Z_{11_{muscle}} - Z_{12_{muscle}} \right] \\ &= \frac{\rho_{muscle}}{4\pi h_{muscle}} \ln \left[\frac{r_{AB}}{r_A} \frac{r_{AB}}{r_B} \frac{r_{AD}}{r_{AC}} \frac{r_{BC}}{r_{BD}} \right] \end{aligned} \tag{6}$$

$$\begin{aligned} Z_{R_{muscle}} &= \frac{1}{2} \left[Z_{22_{muscle}} - Z_{12_{muscle}} \right] \\ &= \frac{\rho_{muscle}}{4\pi h_{muscle}} \ln \left[\frac{r_{CD}}{r_C} \frac{r_{CD}}{r_D} \frac{r_{AD}}{r_{AC}} \frac{r_{BC}}{r_{BD}} \right] \end{aligned} \tag{7}$$

$$Z_{0_{muscle}} = Z_{21_{muscle}} = \frac{\rho_{muscle}}{2\pi h_{muscle}} \ln \left[\frac{r_{AC}}{r_{AD}} \frac{r_{BD}}{r_{BC}} \right] \tag{8}$$

C. Return Path Capacitance

In Human Body Communication, the return path capacitance plays a vital role to establish the overall channel response. For example, in Capacitive HBC, body provides the forward path

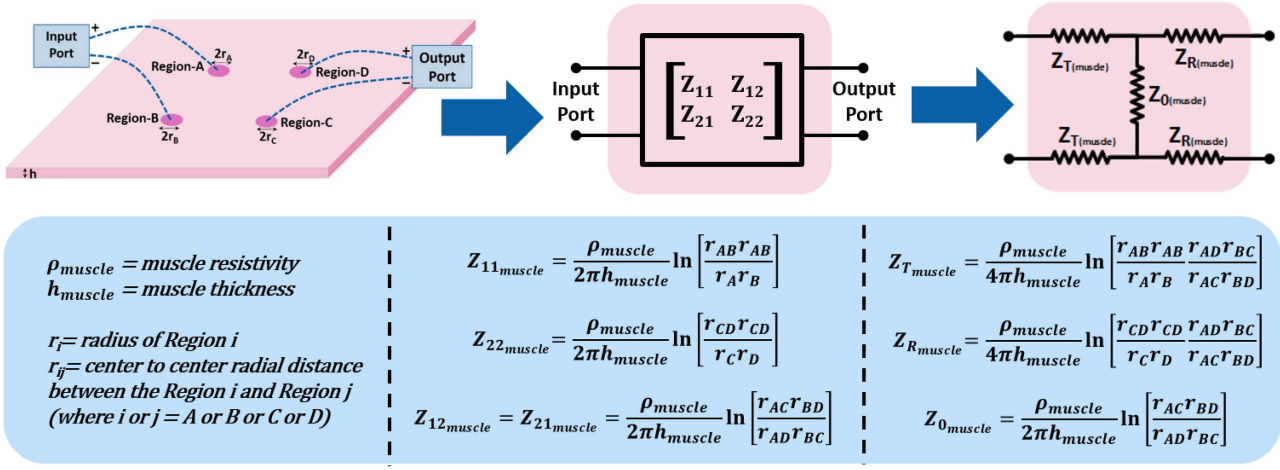

Fig. 4. The equivalent two port representation of muscle layer with all the Z-parameters of the network representing the geometrical and electrical properties of the muscle layer as impedance parameters.

for the signal transmission and the return path for the signal is formed by the electrode to Earth-ground capacitance (return path capacitance) associated with the floating electrode of the transmitter and receiver. Return path capacitances have a much higher impedance compared to the forward path body impedance. Due to the presence of a high impedance return path, the overall channel response in Capacitive HBC is primarily determined by the value of return path capacitances associated with the floating electrodes [8]. Unlike Capacitive HBC, Galvanic HBC [Fig. 1(b)] uses a pair of electrodes to inject and receive signals. As both the Tx-Rx electrodes stay in contact with the body, Galvanic HBC forms a more complex return path capacitive network which affects the overall channel response drastically. Inclusion of in-body parameters, such as lumped impedance of skin and muscle in the model helps to characterize the in-body signal path whereas inclusion of return path or parasitic capacitance to the model helps to characterize the outer-body signal path. Multiple tissue layers can also be included to maximize the accuracy of the in-body return path [13], [14] but at the cost of computational complexity. In EQS frequency regime, most of the signal travels through the conductive muscle layer. Therefore, a Bio-physical model considering skin and muscle layer for the in-body path with the return path capacitance for the outer-body path provides enough accuracy for fast and easy computation. Adding proper return path capacitances to the Bio-physical model is an absolute necessity and improves the accuracy of the model.

According to the study in [32], for a circular electrode of radius r and thickness h ($h \ll r$), the effective *self-capacitance* (Capacitance with respect to the Earth-ground) is approximately equal to $8\epsilon_0 r$. Due to the body contact to the electrode, there is an electrode to Earth-Ground capacitance through the body; we call it C_{body} [8]. Now, C_{self}, C_{body} along with any extra capacitance C_{extra} added to the electrode node because of transmitter or receiver connection, all together act as a return path capacitance of that electrode. Therefore, for an electrode, the value of the return path capacitance associated with it is given by (9).

$$C_{ret} = C_{self} + C_{extra} + C_{body} \tag{9}$$

D. Complete Bio-Physical Model

The complete proposed Bio-physical model of Galvanic HBC is shown in Fig. 5. The portion of the skin tissue layer between the muscle tissue layer and the electrode has been replaced using an equivalent RC network. The value of the capacitances and resistances are determined by the corresponding electrode area and thickness of the skin layer. The frequency dependent parameters such as dielectric constant and conductivity are taken from [15], [16]. In case of the muscle tissue layer, electrical properties of muscle, thickness, and the geometric position of the transmitter and receiver electrodes determine the values of impedance $Z_{T_{muscle}}$, $Z_{R_{muscle}}$ and $Z_{0_{muscle}}$ as expressed by (6), (7) and (8) respectively. $C_{ret(Tx+)}$ and $C_{ret(Tx-)}$ are the return path capacitances associated with the transmitting electrodes while $C_{ret(Rx+)}$ and $C_{ret(Rx-)}$ are the return path capacitances associated with the receiving electrodes. The other ends of all the return path capacitances are connected to the Earth-ground which forms a signal path between the transmitter and receiver outside of the human body.

IV. Symmetric or Balanced Galvanic Channel

A symmetric or balanced condition of Galvanic channel occurs when both the pairs of transmitting and receiving electrodes possess identical size and shape with equal return path capacitances such that $C_{ret(Tx+)} = C_{ret(Tx-)}$ and $C_{ret(Rx+)} = C_{ret(Rx-)}$. Balanced condition in Galvanic HBC channel provides a lot more flexibility to formulate the channel response using a simple mathematical expression. Fig. 6 shows a balanced galvanic arrangement with channel length d and electrode separation s. Angle θ represents the angular position of the receiver with respect to the transmitter. Due to the identical electrodes, we can consider all the skin capacitances are equal to C_{skin} and resistances are equal to R_{skin}. While the return path capacitances associated to each of the electrodes are equal to C_{ret}. Using appropriate geometric distances (6)–(8) i.e. the impedance parameters $Z_{T_{muscle}}$, $Z_{R_{muscle}}$ and $Z_{0_{muscle}}$ of the muscle layer can be represented as a function of s, d and θ; such

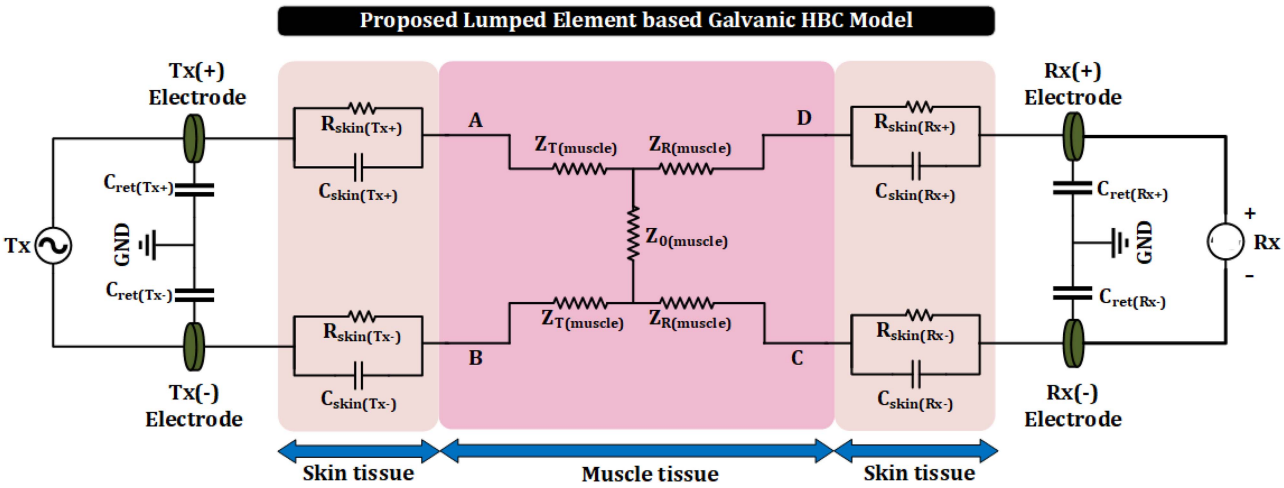

Fig. 5. The complete Bio-physical model of Galvanic HBC which represents the skin and muscle tissue layer with its equivalent lumped impedance.

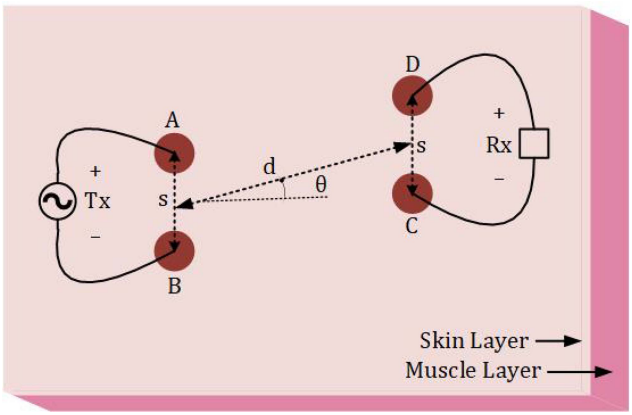

Fig. 6. A pictorial representation of balanced Galvanic HBC with transmitting and receiving electrode separation *s*, channel length *d* and receiver's angular position θ with respect to Tx.

as

$$Z_{T_{muscle}} = \frac{\rho_{muscle}}{4\pi h_{muscle}} \ln\left[\frac{s^2}{r^2}\frac{d^2}{\sqrt{(d^2+s^2)^2-(2sd\sin\theta)^2}}\right] = \frac{\rho_{muscle}}{4\pi h_{muscle}} \ln\left[\frac{s^2}{r^2}\frac{1}{\sqrt{(1+\frac{s^2}{d^2})^2-(\frac{2s}{d}\sin\theta)^2}}\right] \tag{10}$$

$$Z_{R_{muscle}} = \frac{\rho_{muscle}}{4\pi h_{muscle}} \ln\left[\frac{s^2}{r^2}\frac{d^2}{\sqrt{(d^2+s^2)^2-(2sd\sin\theta)^2}}\right] = \frac{\rho_{muscle}}{4\pi h_{muscle}} \ln\left[\frac{s^2}{r^2}\frac{1}{\sqrt{(1+\frac{s^2}{d^2})^2-(\frac{2s}{d}\sin\theta)^2}}\right] \tag{11}$$

$$Z_{0_{muscle}} = \frac{\rho_{muscle}}{2\pi h_{muscle}} \ln\left[\frac{\sqrt{(d^2+s^2)^2-(2sd\sin\theta)^2}}{d^2}\right] = \frac{\rho_{muscle}}{2\pi h_{muscle}} \ln\left[\sqrt{\left(1+\frac{s^2}{d^2}\right)^2-\left(\frac{2s}{d}\sin\theta\right)^2}\right] \tag{12}$$

where,we have considered, electrode radius $r_A = r_B = r_C = r_D = r$; electrode pair separation $r_{AB} = r_{CD} = s$; channel length $r_{AD} = r_{BC} = d$; $r_{AC} = \sqrt{d^2+s^2-2sd\sin\theta}$ and $r_{BD} = \sqrt{d^2+s^2+2sd\sin\theta}$. The expressions of r_{AC} and r_{BD} are calculated by using the properties of triangle in trigonometry. From (10), (11) and (12) we can conclude that for a fixed θ, as d increases, $Z_{T_{muscle}}$ and $Z_{R_{muscle}}$ increases while $Z_{0_{muscle}}$ decreases. Similarly, for a fixed channel length d, as $|\theta|$ $(0 \le |\theta| \le \frac{\pi}{2})$ increases $Z_{T_{muscle}}$ and $Z_{R_{muscle}}$ increases while $Z_{0_{muscle}}$ decreases.

In Voltage-Mode Human Body Communication [8], [33], the impedance provided by the return path capacitance is much higher than the impedance of the body in the signal path. So, the loading effect at the receiver side, due to the presence of return path capacitances is negligible. Therefore, considering negligible loading effect, the transfer function of the balanced Galvanic HBC channel i.e. receiver to transmitter voltage ratio can be expressed with the help of (48) of Appendix B, by replacing impedance Z_0 with $Z_{0_{muscle}}$ and impedance Z_T with $(Z_{skin} + Z_{T_{muscle}})$, such that

$$H(s)_{bal} = \frac{Z_{0_{muscle}}}{Z_{0_{muscle}} + 2[Z_{skin} + Z_{T_{muscle}}]} = \frac{R_{muscle}}{2Z_{skin} + R_{muscle}} \times \left[\frac{\ln[\sqrt{(1+\frac{s^2}{d^2})^2-(\frac{2s}{d}\sin\theta)^2}]}{\ln[\frac{s^2}{r^2}]}\right] \tag{13}$$

where, $R_{muscle} = Z_{0_{muscle}} + 2Z_{T_{muscle}} = Z_{11_{muscle}} = \frac{\rho_{muscle}}{2\pi h_{muscle}} \ln[\frac{s^2}{r^2}]$. The first factor of (13) comes from the voltage division between the skin and muscle layer, whereas the second factor comes from the geometry dependent loss due to the

relative position of the receiving electrodes with respect to the transmitting electrodes. The transfer function (13) can be simplified further into (14), such that

$$H(s)_{bal} = \left[\frac{R_{muscle}}{2R_{skin}}\right] \times \left[\frac{1 + sC_{skin}R_{skin}}{1 + \frac{1}{2}sC_{skin}R_{muscle}}\right] \times \left[\frac{\ln[\sqrt{(1+\frac{s^2}{d^2}) - (\frac{2s}{d}\sin\theta)^2}]}{\ln[\frac{s^2}{r^2}]}\right] \quad (14)$$

where, we consider $R_{skin} \gg R_{muscle}$ and $2R_{skin} + R_{muscle} \simeq 2R_{skin}$ [16] in EQS frequency regime. Now using (14) a balanced Galvanic HBC channel gain can be represented as (15), shown at the bottom of this page.

The gain expression $G(f)_{bal}$, represented by (15) contains three different dependencies. The first one is due to the division of the signal between the skin and muscle layer at low frequency range which is mostly insensitive to the frequency. The second one is the frequency dependent dependency which becomes effective at a frequency higher than a few kHz. The last one represents the dependency of the channel response on channel length, electrode separation and the angular position of the receiver which can be called the channel response due to the channel geometry and shape. The last part of the gain expression also tells the increase in channel loss as d and $|\theta|$ $(0 \leq |\theta| \leq \frac{\pi}{2})$ increases which is due to the reduction of impedance $Z_{0_{muscle}}$ in the proposed model.

To validate the gain expression, the channel response obtained using (15) has been compared to the channel response obtained from numerical EM simulation. For this purpose, we have considered a planar structure (200 cm × 200 cm) of skin and muscle (1 cm thick) layer and simulated the model in Ansys HFSS, a Finite Element Analysis (FEA) tool. The simulation model used is shown in Fig. 7(a). To simulate galvanic excitation, two copper electrodes are placed at the center of the structure and a 1 Volt lumped port excitation is provided between them. The skin-muscle block is surrounded by an air-box, with a radiation boundary set at its outside surface. Path loss is determined by measuring electric field values at a desired receiver position on the skin-air boundary, and integrating electric field across a line that represents the separation between receiver electrodes. We considered three types of circular electrodes with radii 1 cm, 2 cm, 3 cm for each comparison with electrode separation 10 cm center to center in all cases. The comparative plots in Fig. 7(b) and Fig. 7(c) show that the proposed model is able to obtain the galvanic response on a planar structure with an error margin of less than 5 percent. The sharp voltage drop near the electrode edge in Fig. 7(b) which introduces mismatch between the simulation results and proposed model is due to the finite electrode size which can't be neglected when the channel length is smaller than the electrode radius.

V. Saturation of Galvanic Channel Response for an Asymmetric or Unbalanced Channel

An asymmetric or unbalanced condition of galvanic channel occurs when both the pairs of transmitting and receiving electrodes possess mismatch due to the presence of unequal return path capacitances such that $C_{ret(Tx+)} \neq C_{ret(Tx-)}$ and/or $C_{ret(Rx+)} \neq C_{ret(Rx-)}$. In the previous section, we have found the galvanic channel response considering a balanced or symmetric HBC channel. But in most cases, the balanced nature of the HBC channel is not preserved due to the mismatch in the return path capacitances at the transmitter and receiver electrode pair. Equation (13) shows, under the balanced scenario that the received voltage is proportional to the muscle impedance $Z_{0_{muscle}}$. At longer channel length d or at higher θ, $Z_{0_{muscle}}$ tends to zero leading to very small or almost zero received voltage. But in case of the unbalanced channel, due to the signal flow through the return path capacitances via Earth-ground, the received voltage saturates to a fixed value when $Z_{0_{muscle}}$ reduces below a certain value. In this section, we have found the limiting value of the channel response for a very long unbalanced/asymmetric channel excitation and termination.

In case of a very long body channel with a complicated geometry, we can consider the electrode distances r_{AC}, r_{AD}, r_{BC} and r_{BD} shown in Fig. 6 are approximately equal to the effective channel length d $(\gg s)$ which changes (10), (11) and (12) into (16), (17) and (18) respectively.

$$Z_{T_{muscle}} = \frac{\rho_{muscle}}{4\pi h_{muscle}} \ln\left[\frac{s^2}{r^2}\right] \quad (16)$$

$$Z_{R_{muscle}} = \frac{\rho_{muscle}}{4\pi h_{muscle}} \ln\left[\frac{s^2}{r^2}\right] \quad (17)$$

$$Z_{0_{muscle}} = \frac{\rho_{muscle}}{2\pi h_{muscle}} \ln(1) = 0 \quad (18)$$

Now, with extremely low or zero $Z_{0_{muscle}}$ impedance, the received potential becomes a function of input common-mode potential$(V_{TX_{CM}})$ and the mismatch in the return path capacitances present at the transmitting and receiving side as derived in Appendix B. Therefore, the transfer function of a Galvanic HBC with an unbalanced channel can be represented using (52) of Appendix B by replacing Z_R with $(Z_{skin} + Z_{R_{muscle}})$.

$$\begin{aligned} H(s)_{unb} &= \frac{1}{2}\left(\frac{\Delta C_T}{\Sigma C_T}\right)[s(Z_{skin} + Z_{R_{muscle}})(\Delta C_R)] \\ &= \frac{1}{2}\left(\frac{\Delta C_T}{\Sigma C_T}\right)\left[s(Z_{skin} + \frac{1}{2}R_{muscle})(\Delta C_R)\right] \\ &= \frac{1}{2}\left(\frac{\Delta C_T}{\Sigma C_T}\right)\left[\frac{1 + \frac{1}{2}sC_{skin}R_{muscle}}{1 + sC_{skin}R_{skin}}\right]s \\ &\quad \times R_{skin}(\Delta C_R) \end{aligned} \quad (19)$$

$$G(f)_{bal} = 20\log\left[\frac{R_{muscle}}{2R_{skin}}\right] + 10\log\left[\frac{1 + (2\pi f C_{skin}R_{skin})^2}{1 + (\pi f C_{skin}R_{muscle})^2}\right] + 20\log\left[\frac{\left|\ln\left(\sqrt{(1+\frac{s^2}{d^2}) - (\frac{2s}{d}\sin\theta)^2}\right)\right|}{\left|\ln\left(\frac{s^2}{r^2}\right)\right|}\right] \quad (15)$$

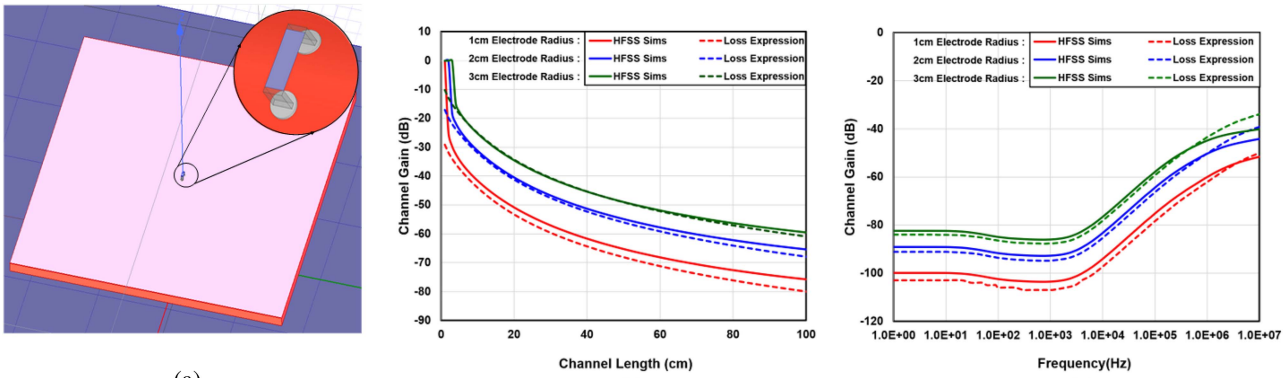

Fig. 7. Comparative results of the simulation data with derived channel gain expression obtained from the proposed Bio-physical model. (a) Shows a planner structure sketching of skin and muscle layers used in FEM simulation with electrodes connected to the center of the structure, (b) Represents the comparative plot of channel gain vs channel length for three different electrode sizes at a fixed 400 kHz frequency of operation; (c) Represents the comparative plot of channel gain vs frequency for three different electrode sizes for a fixed 50 cm channel length.

where, we have considered $\Delta C_T (= C_{ret(Tx-)} - C_{ret(Tx+)})$ is the mismatch in the return path capacitance and $\Sigma C_T (= C_{ret(Tx+)} + C_{ret(Tx-)})$ is the total return path capacitance at transmitter side; $\Delta C_R (= C_{ret(Rx-)} - C_{ret(Rx+)})$ is the mismatch in the return path capacitance at receiver side. We also considered, $R_{skin} \gg \frac{1}{2} R_{muscle}$ and $R_{skin} + \frac{1}{2} R_{muscle} \simeq R_{skin}$ which is true up to 1 MHz frequency as shown in [16].

In the sub-MHz frequency range it is seen that $1 \ll sC_{skin}R_{skin}$ and $1 \gg \frac{1}{2} sC_{skin}R_{muscle}$ [15], [16]. Therefore, the transfer function can be further reduced to (20).

$$H(s)_{unb} = \frac{1}{2}\left(\frac{\Delta C_T}{\Sigma C_T}\right)\left(\frac{\Delta C_R}{C_{skin}}\right) \tag{20}$$

Using (20), channel gain can be represented as

$$G(f)_{unb} = 20\log\left[\frac{1}{2}\left(\frac{\Delta C_T}{\Sigma C_T}\right)\left(\frac{\Delta C_R}{C_{skin}}\right)\right] \tag{21}$$

From (21) it is seen that, Galvanic channel response for a long and unbalanced channel is a function of mismatch in return path capacitances in EQS frequency region. More specifically, there has to be a mismatch in return path capacitance at both the transmitter and receiver side($\Delta C_T \neq 0$ and $\Delta C_R \neq 0$) to obtain a non-zero received voltage. Mismatch at the transmitter side introduces a common-mode (CM) signal from the differential mode input. That CM gets converted again to a differential-mode (DM) at the receiver side due to the mismatch present in the receiver electrodes. The more the mismatch product the less the signal loss is.

VI. Extending the Concept for Cylindrical Structure

In the previous two sections we have formulated the Galvanic HBC channel response considering a planar structure of skin and muscle layer. But due to the complex structure of the human body, a planar structure is not enough to understand the signal loss around the body. In this section, we extend the concept of the planar structure to a cylindrical body structure, and obtain electric field and channel response data through EM simulations in HFSS. The simulated crossed-cylindrical dummy, which is more similar to the human body geometry, but it is still quite simplified, with an external skin layer and internal muscle mass are shown in Fig. 8. For the crossed-cylindrical model, average human body dimensions are assumed, with a 4 mm thick skin, and body and arm radii as 14 cm and 6 cm respectively. We start with the E-field around the body for different type of excitations, namely capacitive, balanced galvanic and unbalanced galvanic. For all three cases, a 1 Volt lumped port excitation is provided between two transmitter electrodes. For capacitive, one electrode is left floating, simulating a floating ground. For unbalanced galvanic, extended metal plates are connected to one of the electrodes, to simulate asymmetry. The purpose of these simulations is to verify and validate whether the previously gained intuitions developed through planar structure extend to a scenario much closer to a real human body.

The strength of the E-Field around the cylindrical structure for three different excitation modes are also shown in Fig. 8. The E-field pattern around the cylindrical structure with a transmitter connected capacitively is shown in Fig. 8(a). From the field pattern, it is seen that the E-field is available everywhere around the body which ensures relatively less variant channel loss for capacitive HBC. Fig. 8(b) shows the E-field pattern of a balanced Galvanic HBC. Here the E-field is restricted to a smaller region and dies out rapidly as distance from the transmitter increases. That is why channel loss in balanced Galvanic HBC increases with channel length. Fig. 8(c) shows the field pattern of an unbalanced Galvanic HBC. Here, the unbalanced scenario is created by adding extra metallic plates to one of the electrodes. The plates are supposed to emulate a grounded chassis of real-world devices, e.g. the metallic chassis of an oscilloscope. Adding additional ground plates this way, helps us to control the amount of asymmetry in the unbalanced galvanic cases. In this case, the voltage distributions between the transmitting electrodes happen unequally due to the unequal return path capacitance to the respective electrodes with respect to Earth-ground. The unequal voltages at the transmitting electrodes introduce CM potential

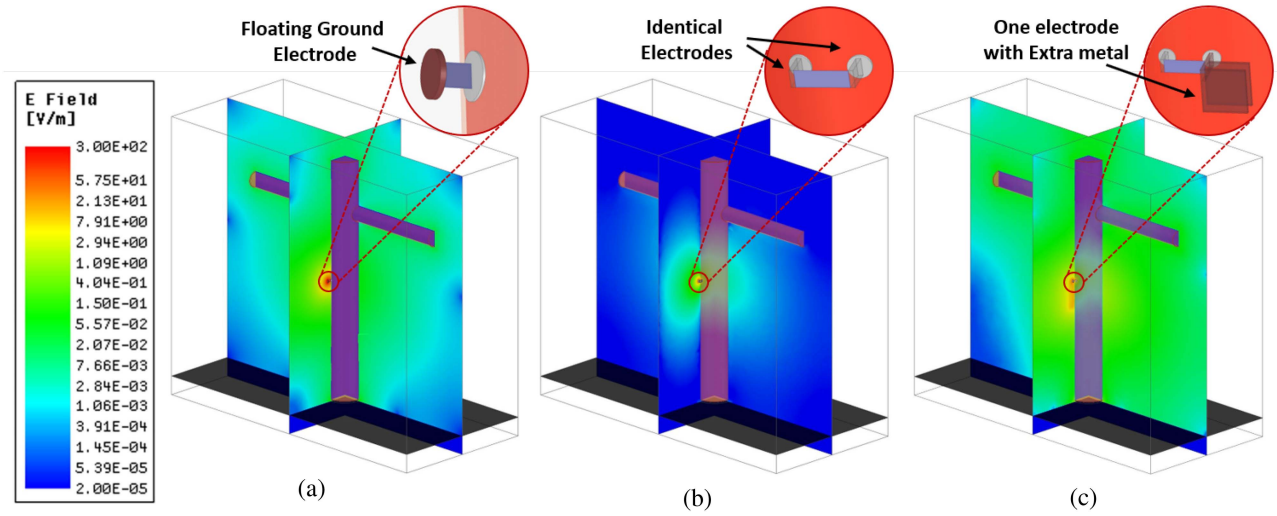

Fig. 8. E-Field around the human body with (a) Capacitive Excitation, (b) Balanced Galvanic Excitation and (c) Unbalanced Galvanic Excitation.

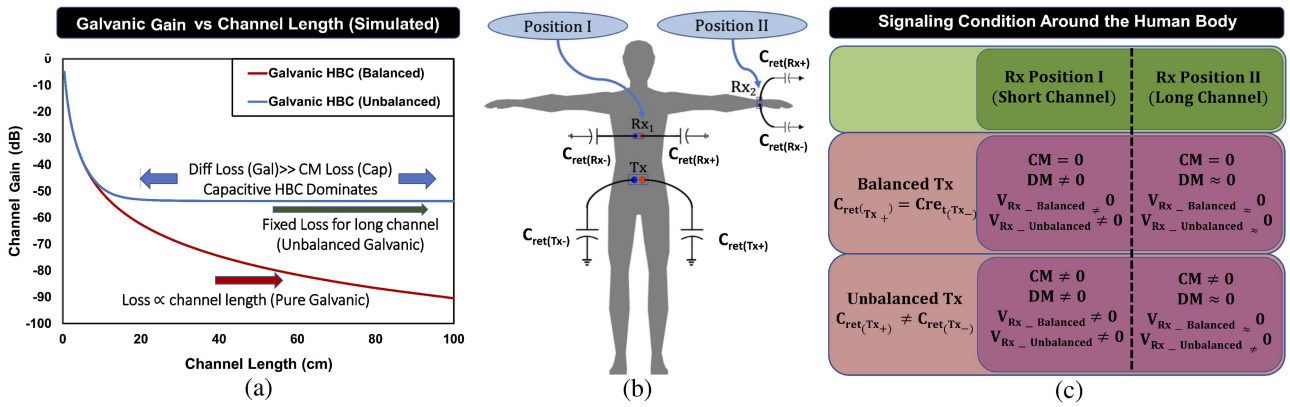

Fig. 9. (a) The Simulation results of the distance dependent galvanic channel gain with Balanced or Unbalanced Tx-Rx pair; (b) and (c) shows the signaling condition around the human body in a galvanic arrangement considering short and long channel length.

and that CM potential raises the overall body potential which can be picked up anywhere around the body. Because of the CM potential, the E-Field is not restricted to a smaller region like the balanced transmission shown in Fig. 8(b). From the E-field pattern, it can also be concluded that at a longer channel length an unbalanced Galvanic HBC acts like capacitive HBC where the channel response is independent of channel length. At shorter channel length, the received voltage is due to the DM voltage as well as CM voltage but the voltage due to the DM dominates, and that makes the received voltage a function of channel length. At longer channel length DM voltage becomes very small and only the CM voltage contributes to the received potential.

Fig. 9(a) shows the simulated galvanic channel response with respect to the channel length. In case of a balanced channel, the loss increases with channel length while in case of an unbalanced channel the loss increases with channel length and saturates to a fixed value for a channel longer than 10 cm. The saturation value and saturation distance are determined by the mismatch present at the receiver and transmitter side as expressed by the (21).

Fig. 9(b) shows different types of signaling conditions depending on the nature of the channel. The channel between the transmitter and the first receiver Rx_1 is considered to be a short channel and the distance between the transmitter and second receiver Rx_2 is considered to be a long channel. The nature of the received signal depending on the balanced or unbalanced conditions are shown in Fig. 9(c).

VII. Measurement Results

In this section, we perform galvanic channel measurements to ascertain the validity of the proposed model.

A. Measurement Setup

The HBC channel response measurement setup with transmitter and receiver connected in galvanic arrangement is shown in Fig. 10. A battery-operated portable signal generator which generates frequency up to 1 MHz is used to generate a sinusoidal signal at 400KHz. At the receiver side, a battery-operated portable spectrum analyzer from 'RF Explorer' is used to capture

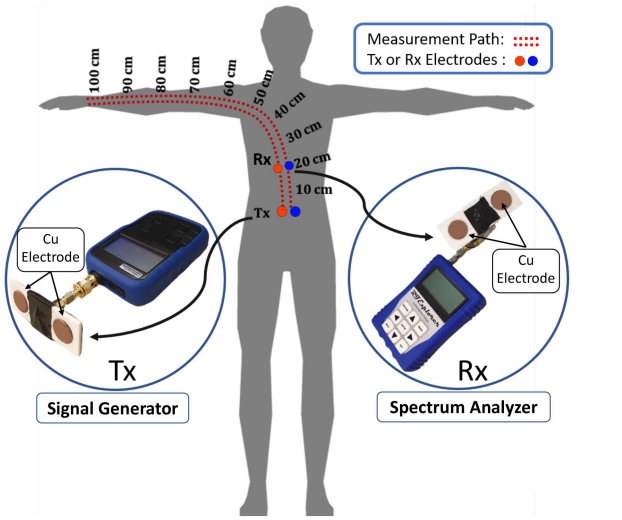

Fig. 10. Diagram showing the position of Tx (fixed at waist) and Rx (moved along the dotted path) during the measurement.

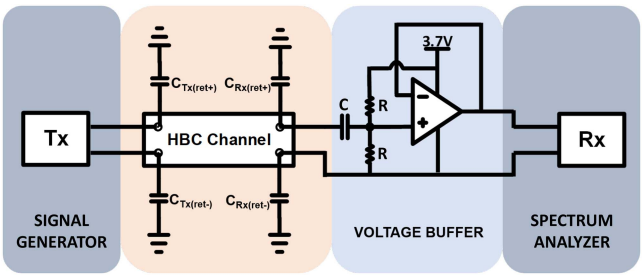

Fig. 11. The measurement circuit diagram.

the signal. To reduce the wireless coupling between Tx and Rx, the electrodes are kept as close as possible to the signal generating or receiving port of these instruments. The connections between the signal generator and receiver with electrodes are made using coaxial SMA connectors to keep the signal shielded from outside noise. Circularly shaped copper metal with radius $1cm$ is used as an electrode. Each electrode pair of Tx and Rx is kept $5cm$ (center to center) apart from each other during the entire measurement process.

B. High Impedance Termination

A portable spectrum analyzer is used here as Rx during measurement. It has 50Ω input impedance which makes a low impedance termination at the receiver side. As described in [8], the low-frequency flat band response is only possible if the channel has a high impedance capacitive termination. A voltage buffer after the receiver electrodes provides the high impedance termination of the HBC channel. A 3.7 V LiPo battery is used to provide supply to the Op-amp. We used a small LiPo battery of size 20 mm x 20 mm x 3 mm to ensure low battery induced capacitance which gets added to the electrode. A resistive divider is used to generate the input bias required to couple the HBC signal as shown in Fig. 11.

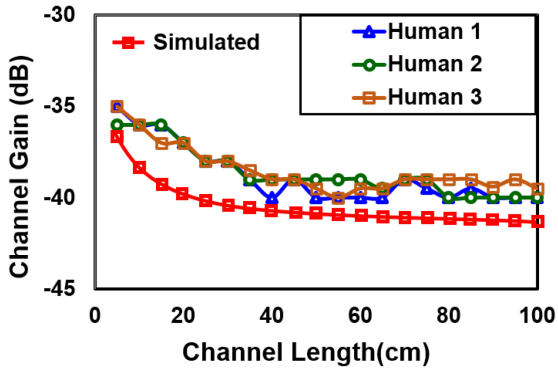

Fig. 12. Comparative plots of simulation and measurement results of capacitive channel gain vs channel length on three different human subjects.

C. Measurement Results of Capacitive HBC Channel

Although the main focus of this paper is to discuss the modeling of Galvanic HBC channel, but to make the understanding better, we have included few measurement results of Capacitive HBC channel. The measurement process as described in [8], is used to measure the distance-dependent channel gain of capacitive HBC, shown in Fig. 12. It is seen that the channel response for capacitive HBC is almost constant and the gain increases slightly due to the inter-device coupling when the devices are very close to each other. We have done the experiment along the path shown in Fig. 10 to minimize the body shadowing effect described in [34]. This measurement result with minimum body shadowing effect helps to have a direct comparison between the Capacitive and Galvanic HBC.

D. Measurement Results of Galvanic HBC Channel

The galvanic channel response measurement is performed on three human subjects with channel length starting from 5 cm to 100 cm. The galvanic transmitter is kept on the waist part of the body with both the electrodes touching the skin. The signal is probed using the receiver along a path as shown in Fig. 10. The measurement results on three different subjects are shown in Fig. 13(a). The measurement results on two different subjects with 2 different electrode sizes (r = 1 cm and 2 cm) are shown in Fig. 13(b). Fig. 13(c) shows the frequency dependent channel response for a 50 cm channel length on three different human subjects. We kept the channel length 50 cm during the gain vs frequency measurement to ensure nominal inter-device coupling.

VIII. Discussion

The heterogeneity of the measurement instrument along with the complex shape of the human body makes the measurement more difficult as described by [22]. If we carefully observe the first two measurement results in Fig. 13(a) and Fig. 13(b), unlike capacitive HBC, for a shorter channel length, loss increases with length and saturates to a constant value for channel length longer than 50 cm. The possible explanation of this kind of

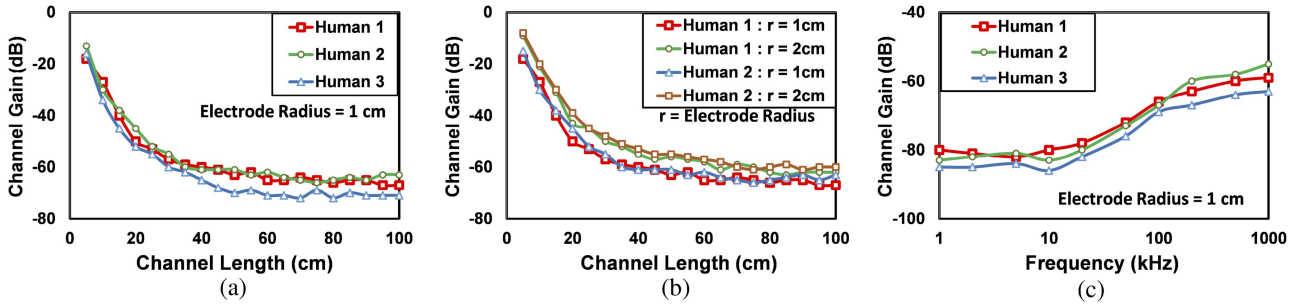

Fig. 13. (a) Galvanic Channel gain vs Channel length plot on three different human subjects with 1 cm electrode radius and 5 cm center to center electrode separation, (b) Galvanic Channel gain vs Channel length plot on two different human subjects with 2 different electrode sizes (1 cm and 2 cm), (c) Galvanic Channel gain vs frequency plot for 50 cm Galvanic Channel on three different subjects with 1 cm electrode radius and 5 cm center to center electrode separation.

measurement results can be traced back to the selection of the transmitter and receiver module. The portable instruments that we used during the measurement, mostly have a metallic casing that is connected to the ground terminal of the device. The coupling between the metallic casing and Earth-ground introduces bigger return capacitance at the negative plate of the Tx and Rx. While using those instruments in galvanic arrangement, the positive electrode encounters smaller electrode to Earth-ground capacitance compare to the negative electrode i.e. $C_{ret(Tx+)} \ll C_{ret(Tx-)}$ and $C_{ret(Rx+)} \ll C_{ret(Rx-)}$. In case of our measurement setup, an independent experiment [32] shows that, the extra capacitance to the negative plate of the galvanic devices is around 10pF-20 pF which is 10 to 20 times more compare to the capacitance present in the positive electrode. The higher return path capacitance in one of the electrodes leads to an asymmetric or unbalanced scenario which helps to hold a fixed loss at longer channel length. Due to the unavailability of a portable as well as a symmetric or balanced transceiver, it is difficult to measure true symmetric galvanic loss. However, the measurement result proves that, due to the presence of capacitive mismatch a Galvanic HBC channel starts to behave like a capacitive HBC channel at longer channel length i.e. length independent channel loss. Most of the previous work on galvanic channel characterization [12], [14], [28], [30] did not discuss the consequences due to the presence of asymmetry in the channel termination. This work shows how the channel behavior changes and affects the overall loss as a function of distance in presence of electrode asymmetry. It is also worth mentioning that for very close channel the model accuracy deteriorates due to the finite electrode size. Therefore, for very close distance channel response, FEM based tool produces more accurate result than this proposed model, which is due to the presence of other second order effect.

IX. Conclusion

This paper presents a unified Bio-physical model to characterize the Galvanic HBC channel in Electro-Quasistatic frequency regime, and captures the effects of in-body and outer-body signal path on channel response. FEM simulation results are used to understand the behavior of the channel response under balanced and unbalanced channel termination. In capacitive HBC, the channel response is mainly determined by the return path capacitance [8] and the loss remains flat throughout the body. Whereas the galvanic loss is highly dependent on the channel length as represented by (15). For a particular device pair, by comparing the gain expression (15) with capacitive gain, we can find the optimal region for each of the modalities. Also, symmetric or balanced galvanic has low leakage as most of the signal confined inside the body within a small region as shown in Fig. 8(b). So, a balanced galvanic channel can be utilized for physically secure communication. We also get to know, any type of input mismatch in galvanic excitation introduces Differential-Mode(DM) signaling with non-zero common-mode(CM). The DM signal reduces as the channel length increases, whereas the CM signal is independent of the channel length and propagates around the body. If the receiver end is balanced i.e. both the receiving electrodes contain equal return path capacitance, the receiver only captures the differential signal available to its electrodes. In case of an unbalanced receiver i.e. with unequal return path capacitance at the receiver electrodes, the receiver captures signal from the differential mode as well as from the common mode. As the differential mode signal reduces with distance, the position of the receiver and the mismatch factor of both the transmitter and receiver decide the overall received signal strength. The received signal is mostly due to the differential signal for very short channel. In case of a long unbalanced channel, the received signal is mostly due to the common-mode to differential mode conversion. In a long unbalanced channel, the channel behavior is dominated by the capacitive HBC, in spite of galvanic excitation and termination.

References

[1] T. G. Zimmerman, "Personal area networks: Near-field intrabody communication," *IBM Syst. J.*, vol. 35, no. 3.4, pp. 609–617, 1996.
[2] X. Wang *et al.*, "A wideband miniaturized implantable antenna for biomedical application at HBC band," in *Proc. Cross Strait Quad-Regional Radio Sci. Wireless Technol. Conf.*, 2018, pp. 1–3.
[3] N. Fahier and W.-C. Fang, "An HBC-based continuous bio-potential system monitoring using 30 MHz OOK modulation," in *Proc. IEEE Biomed. Circuits Syst. Conf.*, 2017, pp. 1–4.
[4] F. Koshiji, R. Urushidate, and K. Koshiji, "Biomedical signal transmission using human body communication," in *Proc. IEEE 36th Int. Perform. Comput. Commun. Conf.*, 2017, pp. 1–2.

[5] J. Wang *et al.*, "Wearable ECG based on impulse-radio-type human body communication," *IEEE Trans. Biomed. Eng.*, vol. 63, no. 9, pp. 1887–1894, Sep. 2016.

[6] D. Das *et al.*, "Enabling covert body area network using electro-quasistatic human body communication," *Sci. Rep.*, vol. 9, no. 1, pp. 1–14, Mar. 2019.

[7] M. Hessar, V. Iyer, and S. Gollakota, "Enabling on-body transmissions with commodity devices," in *Proc. ACM Int. Joint Conf. Pervasive Ubiquitous Comput.*, 2016, pp. 1100–1111.

[8] S. Maity, M. He, M. Nath, D. Das, B. Chatterjee, and S. Sen, "Bio-physical modeling, characterization, and optimization of electro-quasistatic human body communication," *IEEE Trans. Biomed. Eng.*, vol. 66, no. 6, pp. 1791–1802, Jun. 2019.

[9] Y. Nishida *et al.*, "Equivalent circuit model viewed from receiver side in human body communication," *IEEE Trans. Biomed. Circuits Syst.*, vol. 13, no. 4, pp. 746–755, Aug. 2019.

[10] M. S. Wegmueller *et al.*, "Signal transmission by galvanic coupling through the human body," *IEEE Trans. Instrum. Meas.*, vol. 59, no. 4, pp. 963–969, Apr. 2010.

[11] G. Chang *et al.*, "Design considerations of a Sub-50 Mu-W receiver front-end for implantable devices in MedRadio band," in *Proc. 31st Int. Conf. VLSI Des. 17th Int. Conf. Embedded Syst.*, 2018, pp. 329–334.

[12] Y. Song, Q. Hao, K. Zhang, M. Wang, Y. Chu, and B. Kang, "The simulation method of the galvanic coupling intrabody communication with different signal transmission paths," *IEEE Trans. Instrum. Meas.*, vol. 60, no. 4, pp. 1257–1266, Apr. 2011.

[13] J. Mao *et al.*, "A five-tissue-layer human body communication circuit model tunable to individual characteristics," *IEEE Trans. Biomed. Circuits Syst.*, vol. 12, no. 2, pp. 303–312, Apr. 2018.

[14] M. Swaminathan, F. S. Cabrera, J. S. Pujol, U. Muncuk, G. Schirner, and K. R. Chowdhury, "Multi-path model and sensitivity analysis for galvanic coupled intra-body communication through layered tissue," *IEEE Trans. Biomed. Circuits Syst.*, vol. 10, no. 2, pp. 339–351, Apr. 2016.

[15] "Tissue frequency chart IT'IS foundation," [Online]. Available: https://itis.swiss/virtual-population/tissue-properties/database/tissue-frequency-chart/

[16] S. Gabriel, R. W. Lau, and C. Gabriel, "The dielectric properties of biological tissues: II. Measurements in the frequency range 10 Hz to 20 GHz," *Phys. Med. Biol.*, vol. 41, no. 11, pp. 2251–2269, Nov. 1996.

[17] X. M. Chen, P. U. Mak, S. H. Pun, Y. M. Gao, M. I. Vai, and M. Du, "Signal transmission through human muscle for implantable medical devices using galvanic intra-body communication technique," in *Proc. Annu. Int. Conf. IEEE Eng. Med. Biol. Soc.*, 2012, pp. 1651–1654.

[18] S. H. Pun *et al.*, "Quasi-static modeling of human limb for intra-body communications with experiments," *IEEE Trans. Inf. Technol. Biomed.*, vol. 15, no. 6, pp. 870–876, Nov. 2011.

[19] M. S. Wegmueller *et al.*, "An attempt to model the human body as a communication channel," *IEEE Trans. Biomed. Eng.*, vol. 54, no. 10, pp. 1851–1857, Oct. 2007.

[20] D. Ahmed, G. Fischer, and J. Kirchner, "Simulation-based models of the galvanic coupling intra-body communication," in *Proc. IEEE Sensors Appl. Symp.*, 2019, pp. 1–6.

[21] R. Xu, H. Zhu, and J. Yuan, "Electric-field intrabody communication channel modeling with finite-element method," *IEEE Trans. Biomed. Eng.*, vol. 58, no. 3, pp. 705–712, Mar. 2011.

[22] M. A. Callejón *et al.*, "Measurement issues in galvanic intrabody communication: Influence of experimental setup," *IEEE Trans. Biomed. Eng.*, vol. 62, no. 11, pp. 2724–2732, Nov. 2015.

[23] J. Wang, Y. Nishikawa, and T. Shibata, "Analysis of on-body transmission mechanism and characteristic based on an electromagnetic field approach," *IEEE Trans. Microw. Theory Techn.*, vol. 57, no. 10, pp. 2464–2470, Oct. 2009.

[24] E. Reusens *et al.*, "Characterization of on-body communication channel and energy efficient topology design for wireless body area networks," *IEEE Trans. Inf. Technol. Biomed.*, vol. 13, no. 6, pp. 933–945, Nov. 2009.

[25] M. A. Callejón *et al.*, "A parametric computational analysis into galvanic coupling intrabody communication," *IEEE J. Biomed. Health Informat.*, vol. 22, no. 4, pp. 1087–1096, Jul. 2018.

[26] K. Ito and Y. Hotta, "Signal path loss simulation of human arm for galvanic coupling intra-body communication using circuit and finite element method models," in *Proc. IEEE 12th Int. Symp. Auton. Decentralized Syst.*, 2015, pp. 230–235.

[27] N. Cho, J. Yoo, S. Song, J. Lee, S. Jeon, and H. Yoo, "The human body characteristics as a signal transmission medium for intrabody communication," *IEEE Trans. Microw. Theory Techn.*, vol. 55, no. 5, pp. 1080–1086, May 2007.

[28] M. A. Callejón *et al.*, "Distributed circuit modeling of galvanic and capacitive coupling for intrabody communication," *IEEE Trans. Biomed. Eng.*, vol. 59, no. 11, pp. 3263–3269, Nov. 2012.

[29] M. A. Callejon *et al.*, "Study of attenuation and dispersion through the skin in intrabody communications systems," *IEEE Trans. Inf. Technol. Biomed.*, vol. 16, no. 1, pp. 159–165, Jan. 2012.

[30] B. Kibret *et al.*, "Investigation of galvanic-coupled intrabody communication using the human body circuit model," *IEEE J. Biomed. Health Informat.*, vol. 18, no. 4, pp. 1196–1206, Jul. 2014.

[31] J. Bae *et al.*, "The signal transmission mechanism on the surface of human body for body channel communication," *IEEE Trans. Microw. Theory Techn.*, vol. 60, no. 3, pp. 582–593, Mar. 2012.

[32] M. Nath, S. Maity, and S. Sen, "Towards understanding the return path capacitance in capacitive human body communication," *IEEE Trans. Circuits Syst. II: Exp. Briefs*, vol. 67, no. 10, pp. 1879–1883, Oct. 2020.

[33] S. Maity, D. Das, and S. Sen, "Wearable health monitoring using capacitive voltage-mode human body communication," in *Proc. 39th Annu. Int. Conf. IEEE Eng. Med. Biol. Soc.*, 2017, pp. 1–4.

[34] A. Datta *et al.*, "Advanced biophysical model to capture channel variability for EQS capacitive HBC," *IEEE Trans. Biomed. Eng.*, vol. 68, no. 11, pp. 3435–3446, Nov. 2021.